https://doi.org/10.5194/egusphere-2025-4315
Preprint. Discussion started: 17 September 2025

Storm-time Energy Budget in the High Latitude Lower Thermosphere-Ionosphere: Quantification of Energy Exchange and Comparison of Different Drivers in TIE-GCM

Stelios Tourgaidis[1], Dimitrios Baloukidis[1], Theodoros Sarris[1], Stephan Buchert[2], Panagiotis Pirnaris[1], and Kostis Papadakis[3]

[1]Department of Electrical and Computer Engineering, Democritus University of Thrace, Xanthi
[2]Swedish Institute of Space Physics, Uppsala, Sweden
[3]Department of Physics, University of Helsinki, Helsinki, Finland

Correspondence: Stelios Tourgaidis (stourgai@ee.duth.gr)

Abstract. The energy flow and energy balance in the Lower Thermosphere-Ionosphere (LTI) is governed by a number of processes that are driven by interactions between ions, neutrals and electrons. Even though these processes are well understood theoretically, and even though the framework to implement these processes exists in current global circulation models, the energy estimates for the different processes show large discrepancies between models, in large part because of limitations in available data sets. In this study, we explore numerically the energy inputs and energy transfer between ions, neutrals and electrons during the 2015 St. Patrick's day geomagnetic super-storm. We use NCAR's Thermosphere Ionosphere Electrodynamics General Circulation Model, version 2.0 (TIE-GCM 2.0) for estimating energy sources and sinks, energy transfer rates and the energy partitioning between species. Two independent TIE-GCM runs were executed: the first one used the Weimer 2005 empirical model, and the second used the Assimilative Mapping of Ionospheric Electrodynamics (AMIE) data assimilative technique. The resulting energy budget and the corresponding partitioning of energy between species are inter-compared between the two runs, before and at the peak of the storm. Discrepancies between the model runs are discussed and the way forward to close the gaps in present knowledge is highlighted.

1 Introduction

Energy flow in the Earth's Lower Thermosphere-Ionosphere (LTI) is a complex process involving collisional interactions between ions, electrons and neutrals (see, e.g., Sarris et al. (2023a) and references therein). A key characteristic of the LTI system is that its energy balance is driven and controlled by external sources of forcing, including solar extreme ultraviolet (EUV) and X-ray irradiance, the solar wind impinging upon the Earth's magnetosphere and energetic particle precipitation. At the same time, upward-penetrating tides and gravity waves continuously deposit energy and momentum from the mesosphere and the troposphere below. During quiet times, or on long-term averages, the main energy input into the LTI is solar radiation, which is absorbed primarily by O_3, O_2, O and CO_2. More specifically, O, the most abundant constituent at about 150 km and above, absorbs solar radiation in EUV, O_2 absorbs far ultraviolet radiation (100-200 nm) at altitudes of about 100-150 km, and O_3

https://doi.org/10.5194/egusphere-2025-4315
Preprint. Discussion started: 17 September 2025

absorbs solar ultraviolet radiation of 200-300 nm at mid-atmospheric altitudes. However, during times of enhanced solar and geomagnetic activity, the main energy input into the LTI is energy from the solar wind impinging upon the Earth's magnetosphere, which can greatly exceed the energy input from solar EUV radiation. Furthermore, during active times, energetic charged particles are accelerated in the magnetosphere and precipitate along magnetic field lines into the auroral regions of the LTI. Energetic Particle Precipitation leads to energy deposition, conductivity changes, and chemical changes in the LTI and below, as the braking of precipitating electrons primarily between 90-200 km via collisions with the neutral atmosphere results in increased thermal plasma and heating, and also in enhanced conductivity within this region. During active times, at high latitudes, Joule heating is the most thermodynamically important process, dissipating energy from the magnetosphere. Joule heating greatly affects the state of the LTI by altering neutral winds, temperatures, composition and densities in a significant way. It is thought that, during active times, the effects of Joule heating on the upper atmosphere are more significant than those of EUV or energetic and auroral particle precipitation (e.g., Zhang et al. (2017)). However, the exact quantification of Joule heating is largely unknown, primarily due to a lack of systematic measurements of all relevant terms contributing to Joule heating (see, e.g., Sarris (2019); Palmroth et al. (2021); Tourgaidis et al. (2025a)), leading to large discrepancies between models. It can thus be stated that Joule heating is among the least known and least quantified processes in the LTI, while being among the most significant ones in terms of the energy budget of the ionosphere-thermosphere system, in particular during active times.

Many studies have examined the energy budget of the ionosphere-thermosphere system through model runs of global circulation models. For example, Killeen et al. (1997), performed estimates of the energy budget in the lower thermosphere, using the NCAR Thermosphere-Ionosphere-General Circulation Model (NCAR-TIGCM). They found that LTI heating and cooling has complex morphological dependencies on latitude, longitude, altitude, geomagnetic activity, and season, and they discussed the altitude dependence of each heating term. At the highest altitudes resolved by TIGCM, they found a significant role by minor species chemistry at 175 km, and significant cooling by adiabatic expansion, NO cooling, and downward heat conduction, whereas at 125 km altitude, they found that direct solar insolation and Joule heating are the most important heating terms. Furthermore, they found an equal cooling role of NO and CO_2, with adiabatic expansion being of significance at high latitudes during summer. At 103 km, the lowest altitudes considered, they found that direct solar insolation, heat conduction, and adiabatic compressional effects dominate the heating, whereas the dominant cooling term at these altitudes was caused by CO_2, radiation, with heat advection and adiabatic expansion in the summer hemisphere playing minor roles. Finally, they found that NO cooling rates can double globally during high levels of geomagnetic activity. In another analysis of the LTI energy partition, Verkhoglyadova et al. (2016) used a combination of empirical models and Global Ionosphere-Thermosphere Model (GITM) (Ridley et al. (2006)) simulations to investigate the heating and cooling rates in the LTI during two moderate storms caused by High-Speed Streams (HSSs) occurred on 22-31 January 2007 and 25 April-2 May 2011, corresponding to the descending phase of solar cycle 23 and the ascending phase of solar cycle 24 respectively. They used different coupling functions to estimate the energy input from the magnetosphere and consequently they calculated the Joule heating rates using empirical formulations. For the cooling rates, they used data from TIMED/SABER satellite, to derive nitric oxide (NO) and carbon dioxide (CO_2) cooling fluxes. They also performed GITM simulations to cross-compare the model outputs to the satellite derived cooling rates and the heating rates based on empirical estimations. For the external driving of the model, they used the Weimer-2005 and the

https://doi.org/10.5194/egusphere-2025-4315
Preprint. Discussion started: 17 September 2025

AMIE formulation for defining the high latitude electric fields. By comparing the GITM outputs to the satellite and empirical data, they found that GITM consistently underestimates NO cooling and auroral heating. Furthermore, Verkhoglyadova et al. (2017), calculated the energy budget of the ionosphere-thermosphere for the storms of March 2013 and 2015 using the GITM model together with observational proxies. GITM was driven by solar wind data, the $F10.7$ index, the OVATION Prime model and the Weimer 2005 model. They found that Joule heating and infrared cooling are likely underestimated in GITM. Despite of significant modeling and observational efforts, the relative contributions from different external drivers to the energy budget in LTI is still a subject of debate, hindering efforts to forecast the state of the LTI, in particular during times of enhanced solar and geomagnetic activity (Heelis and Maute (2020)). At the same time, various mechanisms internal to the LTI convert, transport and redistribute the input energy from the system. Whereas these mechanisms are well-understood theoretically, their quantification also yields large discrepancies between different models.

In this paper, we present model results on the quantification of the various energy dissipation terms in the LTI during the geomagnetic storm of St Patrick's day 2015, as estimated through a simulation using TIE-GCM. Through these simulations, we compare the magnitudes of the hemispherically-integrated heating and cooling terms during the evolution of the storm. In particular, we use two different commonly used models of external driving of the LTI system, an empirical and an assimilative model, and we compare their effects in the energetics and overall energy budget of the LTI. In further detail: in **Section 2.1** we present an overview of the St Patrick's day 2015 geomagnetic storm and studies that have reported observations and modeling results of that event; in **Section 2.2** we describe the TIE-GCM and the simulations that were conducted; and in **Section 2.3** we present in more detail the two different models that are used in this study as external drivers for TIE-GCM to perform the three energy budget inter-comparisons. In **Section 3** we describe the estimation methodology and the formulation that is used to calculate each heating and cooling term, listing the relevant TIE-GCM geophysical observables. In **Section 4** we present the main results and inter-comparisons, estimated from the point of view of the neutrals, the ions and the electrons. In **Section 5** we discuss the results of the simulations, and in **Section 6** we summarize the main findings and conclusions of this study.

2 TIE-GCM simulation of St Patrick's day storm

2.1 St Patrick's day storm

On March 17th, 2015, a severe geomagnetic storm of G4 class was recorded, reaching a minimum Dst index of approximately -223 nT. Known as the 2015 St. Patrick's Day storm, it was the strongest G4 event during Solar Cycle 24, one of only five such storms observed. The storm was triggered by a coronal mass ejection (CME) that occurred around 02:00–02:30 UT on March 15th. An interplanetary shock associated with this CME was detected by the Wind spacecraft at approximately 03:59 UT on March 17th. The onset of the geomagnetic storm at Earth was recorded near 14:00 UT, lasting roughly 18 hours, with G3/G4 level geomagnetic conditions sustained for about 12 hours. A minimum Dst of -190.7 nT was reached at approximately 23:30 UT. A detailed description of the storm can be found in Wu et al. (2016), and references therein. Due to its severity, this event has been extensively investigated: for example, Lyons et al. (2016), Prikryl et al. (2016), and Marsal et al. (2017) studied energy inputs into the high-latitude regions during this event, focusing on the ionospheric disturbances induced by

https://doi.org/10.5194/egusphere-2025-4315
Preprint. Discussion started: 17 September 2025

these energy inputs. Yue et al. (2016), Zhang et al. (2017) and Wei et al. (2019) investigated the observed sub-auroral processes and the related coupling between the ionosphere and the magnetosphere. Zakharenkova et al. (2016) and Dmitriev et al. (2017) studied the response of the neutral winds to the high-latitude energy and momentum inputs and the effects that the storm had on neutral wind patterns. Goldstein et al. (2017) studied ring current dynamics and the enhancement of the plasmasphere. Kanekal et al. (2016) and Hudson et al. (2017) reported the prompt injection and acceleration of energetic electrons. Jaynes et al. (2018) and Ozeke et al. (2020) investigated ULF-driven radial diffusion during this event. Tourgaidis et al. (2025a) calculated the Joule heating rates during this event, using two of the most commonly used physics-based Global Circulation Models (GCM) of the Earth's upper atmosphere: the Global Ionosphere/ Thermosphere Model (GITM) and the Thermosphere-Ionosphere-Electrodynamics General Circulation Model (TIE-GCM), as well as empirical models, and performed detailed comparisons between the various model runs.

An overview of the time evolution of all key parameters relevant to the coupling of the Magnetosphere-Ionosphere-Thermosphere system during this event are presented in **Figure 1**. The Akasofu ϵ parameter (Akasofu, 1981), plotted in panel (a), is a measure of the solar wind energy input into the magnetosphere. It is given as:

$$\epsilon = V_{sw} B^2 sin^4(\theta/2) l_0^2 \tag{1}$$

where V_{sw} is the solar wind speed, B is the interplanetary magnetic field magnitude, $\theta = tan^{-1}(B_y/B_x)$ is the IMF clock angle and l_0 is the characteristic length scale of the magnetopause ($\approx 7R_e$). The Newell coupling function (Newell et al., 2007), plotted in panel (b), is an empirical formula representing the efficiency of solar wind–magnetosphere coupling:

$$\Phi = V_{sw}^{4/3} B_T^{2/3} sin^{8/3}(\theta/2) \tag{2}$$

The Kan-Lee electric field (Kan and Lee, 1979), plotted in panel (c), describes the magnetospheric convection electric field as it maps down to the high latitude ionosphere, giving a description of how energy from the solar wind enters the Earth's magnetosphere and ionosphere. Is expressed as:

$$E_{KL} = V_{sw} B_T \sin^2(\theta/2) \tag{3}$$

where $B_T = \sqrt{B_y^2 + B_x^2}$ is the transverse component of the interplanetary magnetic field (IMF). The SYM-H index, plotted in panel (e), is a high-resolution (1-minute) analog of the Dst (Disturbance storm-time) index, and it represents the strength of the symmetric ring current around Earth. It is used to monitor geomagnetic storm activity with finer temporal resolution than Dst. The AE index (Auroral Electrojet index), plotted in panel (f), quantifies the intensity of auroral zone currents, specifically the eastward (EEJ) and westward (WEJ) electrojets. It is a key indicator of auroral and substorm activity, primarily reflecting variations in the Earth's high-latitude magnetic field caused by enhanced ionospheric currents. The Joule heating deposited onto the ionosphere-thermosphere during this time, calculated via an empirical formulation according to Knipp et al. (2005), is plotted in panel (d). This is given as:

$$JH = 29.41PC + 2.54PC^2 + 0.21Dst + 0.0023Dst^2 \tag{4}$$

https://doi.org/10.5194/egusphere-2025-4315
Preprint. Discussion started: 17 September 2025

where PC and Dst are the Polar Cap and Disturbance Storm Time indices respectively. Together with the empirical formulation of Joule heating according to Knipp et al. (2005), in panel (d) we also plot the Joule heating rate calculated through TIE-GCM runs driven by the Weimer and AMIE models; these will be discussed in more detail in the following.

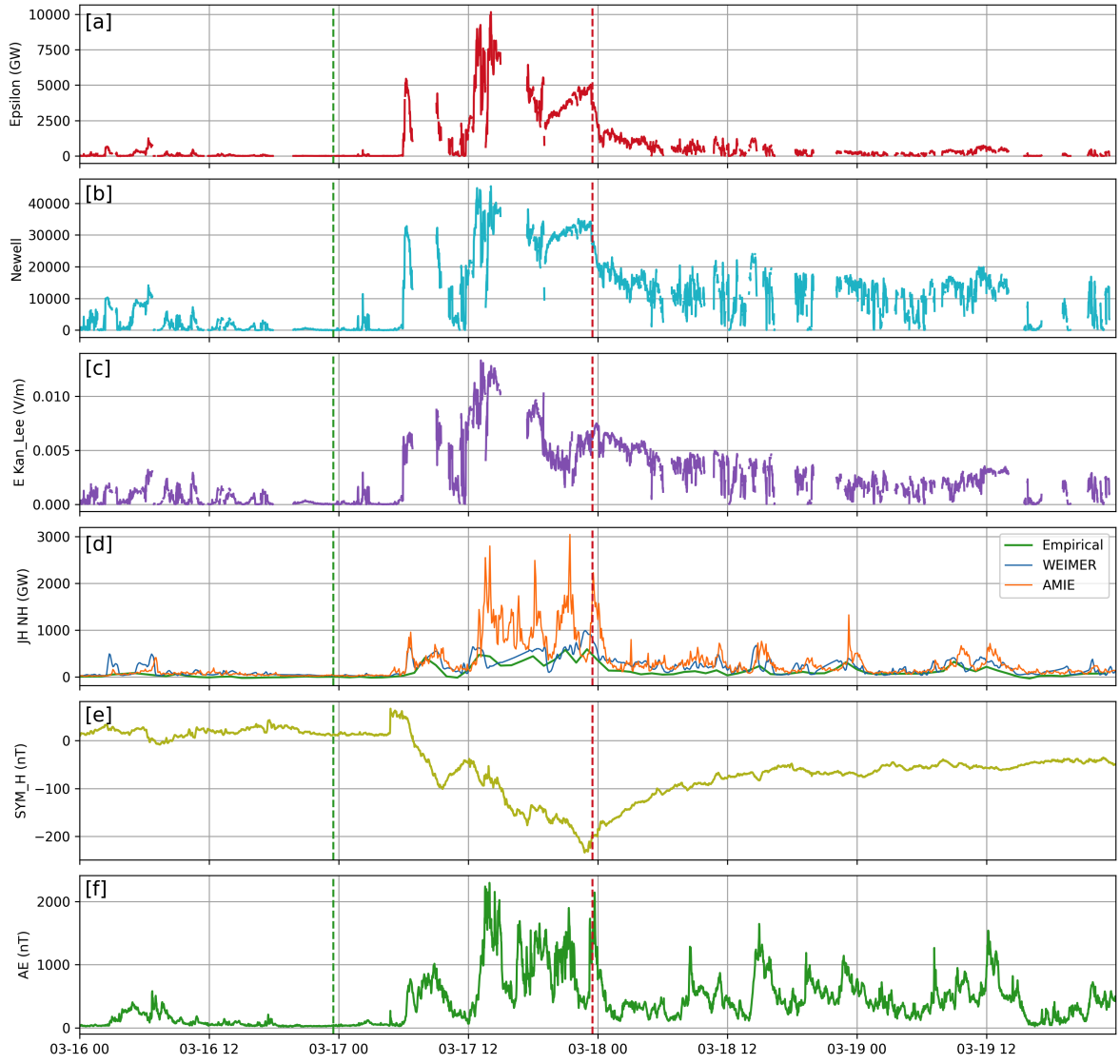

Figure 1. Description of the geomagnetic storm through various parameters: a) Akasofou ϵ parameter, b) Newell coupling function, c) Kan-Lee electric field, d) Joule heating estimates (Empirical, TIE-GCM Weimer, TIE-GCM Amie), e) SYM-H index f) AE index. The red dashed vertical line marks the time of minimum $SYM-H$ index, indicating the peak of the storm. The blue dashed vertical line corresponds to 24 hours before the peak of the storm.

https://doi.org/10.5194/egusphere-2025-4315
Preprint. Discussion started: 17 September 2025

From the panels in **Figure 1** it can be seen that the SYM-H index becomes negative on March 17, 06:53:00 UT, subsequently it presents a local minimum of -101 nT at 09:37:00 UT, another local minimum of -177 nT at 17:28:00 UT, and it reaches its minimum value of -234 nT at 22:47:00 UT. Consequently, SYM-H keeps increasing after the peak of the storm while it continues to be negative for the next four days. The ϵ parameter, which is an estimation of the total power extracted from the solar wind/Interplanetary Magnetic Field into the magnetosphere, presents its first sharp rise to 5453 GW at 06:14:00 UT, its maximum value of 10157 GW at 14:06:00 UT, while around the minimum of the SYM-H index has an elevated value of around 5000 GW. Following on, its values drop rapidly and become comparable to the pre-storm period. The Newell coupling function and the Kan-Lee electric field follow the same trend as the ϵ parameter, with the difference that their values are kept elevated after the storm, with respect to the pre-storm period. The Joule heating estimations through the Knipp et al. (2005) empirical formula and with the WEIMER, are in good agreement, while there are large differences between these model resutls and the Joule heating as calculated by the AMIE run. Finally, regarding the AE index, there are many local maximums during the main phase of the storm and it has high correlation with the Joule heating calculated with the AMIE run. For the following analyses, we chose the time of the peak of the AMIE Joule heating which is closer to the minimum of the SYM-H index, i.e. at 23:30:00 UT of March 17, marked with a dashed vertical red line in **Figure 1**. As a pre-storm baseline timestep we chose one day before, i.e. at 23:30:00 UT of March 16 marked with a dashed blue line. It is noted that the interplanetary coupling functions ϵ, the Newell parameter and the Kan-Lee electric field include gaps in their timeseries resulting from data gaps of the interplanetary magnetic field measurements.

In this paper, using TIE-GCM (see **Section 2.2**), we simulate 4 days around the St. Patrick's day storm, starting from 2 days before and up to 2 days after the time of the minimum Dst index of the event, and we quantify the various energy sources and energy dissipation terms in the Lower Thermosphere - Ionosphere. Energy terms are viewed from the perspective of the neutrals, the ions and the electrons, allowing to monitor the energy transfer between species. We use two different electric potential models as external drivers to TIE-GCM (see **Section 2.3**), and we quantify and cross-compare the variations in the various energy terms based on the different external drivers.

2.2 The Thermosphere - Ionosphere - Electrodynamics General Circulation Model (TIE-GCM)

A global self-consistent simulation of the LTI environment during St. Patrick's day stom was performed using the National Center for Atmospheric Research (NCAR) Thermosphere-Ionosphere-Electrodynamics General Circulation Model (TIE-GCM). TIE-GCM is a three-dimensional global model of the thermosphere and ionosphere system, spanning altitudes from ~ 100 km up to ~ 600 km. TIE-GCM is based on first-principles and, at each simulation time step, solves the momentum, energy and continuity equations for neutral, ion and electron species. In this study, version 2.0 of the TIE-GCM is used in the simulations.

Calculations of the various energy terms were performed at every grid point of TIE-GCM; subsequently, energy terms were integrated across all latitudes and longitudes, as well as across all altitudes. Integrations were performed separately for the Northern and Southern hemispheres. The TIE-GCM grid is pressure defined, thus in order to perform the integration a re-griding procedure was followed to translate the pressure defined grid to altitude defined. After the re-griding procedure,

https://doi.org/10.5194/egusphere-2025-4315
Preprint. Discussion started: 17 September 2025

integrations were performed with a trapezoidal integration scheme, according to equation:

$$\int f(x) \approx \sum([f(x_{k-1}) + f(x_k)]/2) * \Delta x$$

The TIE-GCM uses an imposed electric field model as external driver for the specification of the electric potential at high magnetic latitudes. Two such models are used in this study, and the results from the two runs are inter-compared, as the external specification significantly affects the resulting energy flow. These external drivers are described in further detail in the following section.

2.3 External drivers of TIE-GCM - Electric Potential Models

The thermosphere-ionosphere system is driven externally by high-latitude electric fields as well as auroral precipitation. TIE-GCM is correspondingly driven by models that provide specifications of high-latitude electric fields and particle precipitation. In this study, two different models are used, namely, the Weimer 2005 empirical model (Weimer (2005)), and the Assimilative Mapping of Ionospheric Electrodynamics (AMIE) procedure developed by Richmond and Kamide (1988). The Weimer-2005 empirical model of high-latitude ionospheric electric potential utilizes upstream solar wind and geomagnetic parameters to reconstruct convection patterns. The model is based on measurements of electric fields by the Dynamics Explorer 2 (DE-2) and the Defense Meteorological Satellite Program (DMSP) satellites. Model inputs include the interplanetary magnetic field (IMF) components B_x, B_y, and B_z, as well as the solar wind velocity V_x, which controls the strength of the convection. Additionally, the model incorporates the geomagnetic dipole tilt angle and universal time (UT) to account for seasonal and diurnal asymmetries in the potential pattern. Unlike models based on geomagnetic indices such as Kp or Dst, the Weimer model derives directly from solar wind conditions, enabling a more physically driven and hemispherically resolved specification of ionospheric electrodynamics (Weimer (2005)). This model offers higher spatial resolution and better IMF sensitivity than earlier empirical models like the Heelis et al. (1982) and the Weimer-2001 models. The Assimilative Mapping of Ionospheric Electrodynamics (AMIE) (Richmond and Kamide (1988)) model is a physics-based, data assimilative technique that produces time-dependent maps of high-latitude ionospheric electrodynamics. It assimilates diverse ground (ground magnetometers, ionospheric radars, incoherent scatter radars) and space-based observations. In addition to convection maps, AMIE provides conductivity, ionospheric and field-aligned current estimations in a self-consisting physics-based framework.

3 Estimation Methodology

The energy state and energy balance of the LTI is determined by a number of processes that result in the storage, transport, and transformation of energy into various forms. These processes are governed by collisional interactions between species that determine the energy transfer between ions, neutrals and electrons, as well as by radiative heating due to EUV radiation and radiative cooling due to species such as CO_2, NO and $O(^3P)$. A schematic diagram of the energy flow and the associated processes and pathways in the LTI system is given in **Figure 2**. In this figure, the transfer of energy towards and between the neutral species, ionized species and electrons of the thermosphere-ionosphere system is shown with arrows, as marked. These

https://doi.org/10.5194/egusphere-2025-4315
Preprint. Discussion started: 17 September 2025

processes include: Joule heating, which is deposited to the neutrals and the ions; energy deposition from energetic precipitating protons, which deposit energy directly to the neutrals; energy deposition from energetic precipitating electrons, which deposit energy to the ionospheric electrons; EUV radiation, considered the most significant energy source during quiet times, which heats both the electrons and the neutrals; heat exchange due to temperature differences between: ions and neutrals, ions and electrons, electrons and neutrals; molecular diffusion at higher altitudes; chemical processes related to ion chemistry; heating due to O_2 recombination; photoelectron heating; horizontal diffusion; eddy diffusion, occurring primarily at regions closer to the mesosphere; horizontal advection; and adiabatic heating due to the vertical motion of neutral gases. The most significant radiative cooling terms in the thermosphere include CO_2 and NO, and to a smaller extent $O(^3P)$. Finally, a cooling term is conduction to the middle atmosphere. The processes that are calculated in TIE-GCM are marked with boxes having a solid outline, whereas processes that are not calculated and are thus not presented herein are marked with dashed outlines.

In this study, TIE-GCM is used to estimate numerically each of the energy flow process shown in **Figure 2**. Each of the processes shown in this figure is discussed in more detail in the following section. The equations used and the overall estimation methodology are based on Daedalus MASE (Mission Assessment through Simulation Exercise) (Sarris et al. (2023b)), which is an open-source package of scientific analysis tools aimed at research in the Lower Thermosphere-Ionosphere (LTI). Daedalus MASE was created with the purpose to assess the performance and demonstrate closure of the mission objectives of Daedalus (Sarris et al. (2020)), a mission concept targeting to perform in-situ measurements in the LTI. owever, through its successful usage as a mission-simulator toolset, Daedalus MASE has evolved to encompass numerous capabilities related to LTI science and modeling.

https://doi.org/10.5194/egusphere-2025-4315
Preprint. Discussion started: 17 September 2025

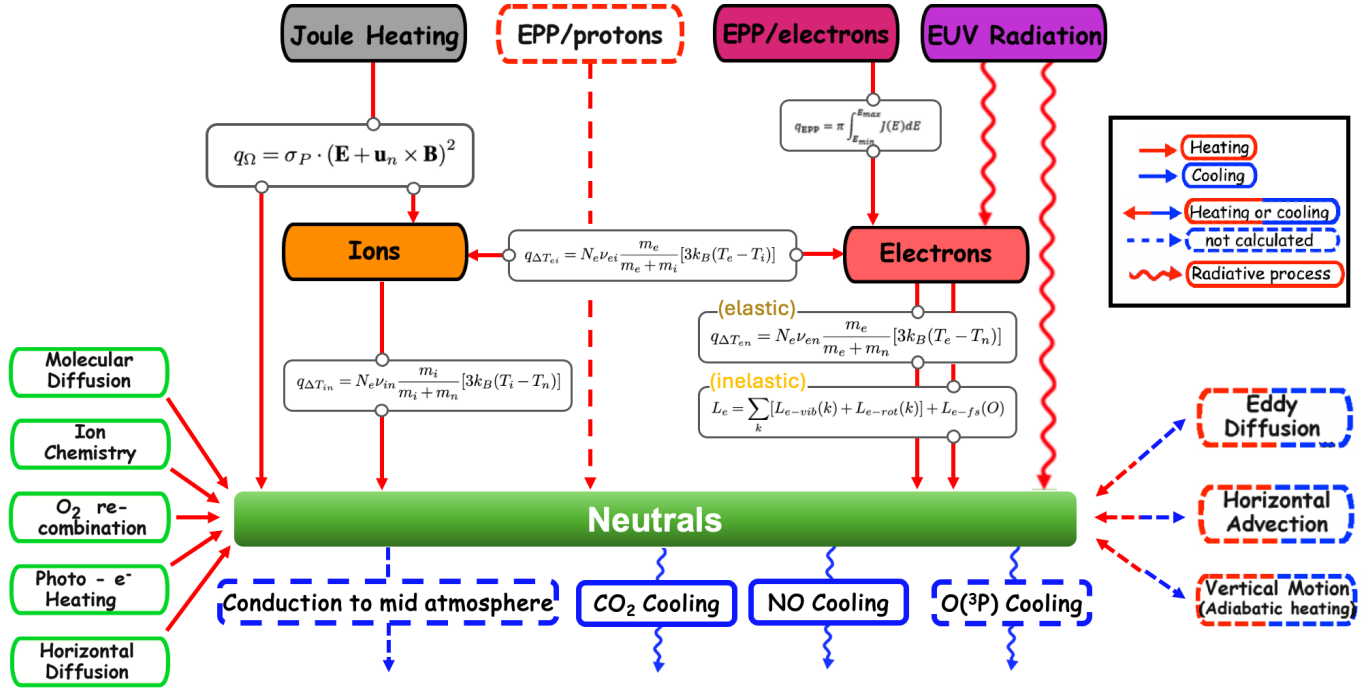

Figure 2. Energy flow in the Lower-Thermosphere-Ionosphere system.

The calculations of the energy transfer and energy dissipation terms are based on calculations of a comprehensive list of geophysical parameters (or physical quantities) of the LTI, which are obtained through a TIE-GCM simulation of the solar storm of St. Patrick's day, March 2015. These geophysical observables include: **(a)** Plasma (ionosphere) parameters: Ion Drift velocity vector ($\mathbf{v}_i$), Ion Temperature (T_i), Electron Temperature (T_e), Ion Number Density (N_i), Electron Number Density (N_e), Ion Composition (n_{ix}); **(b)** Neutral (thermosphere) parameters: Neutral Wind Velocity vector ($\mathbf{u}_n$), Neutral Mass Density (ρ), Neutral Temperature (T_n), Neutral Composition (n_{nx}), and **(c)** LTI fields: the Magnetic Field vector (**B**), and the Electric Field vector (**E**). In the following section, each of the energy flow terms of Figure 2 is described in further detail, including an overview of the theory and the main assumptions that are used in their derivation in TIE-GCM.

3.1 Heating and Cooling Rates

3.1.1 Joule heating

Joule heating is a major heat dissipation process in the LTI, particularly during active times. Joule heating is caused by collisions between ions and neutrals in the presence of a relative drift between the two (Vasyliūnas and Song (2005)). Ion-neutral collisions tend to drive the neutral gas in a similar convection pattern to that of the ions, which with time also generates kinetic energy (Codrescu et al. (1995); Richmond (1995)). The Joule heating estimation methodology based on TIE-GCM outputs is

https://doi.org/10.5194/egusphere-2025-4315
Preprint. Discussion started: 17 September 2025

discussed in further detail in Tourgaidis et al. (2025a), who simulated Joule heating during several days around the superstorm of St. Patrick's day, 2015. Generally, Joule heating is deposited directly into the neutral gas and also heats the ions. In turn, the ions are transferring heat to the neutral gas, as is further discussed below. The Joule heating rate per unit volume, q_{Joule}, is represented as:

$$q_{Joule} = \sigma_P \cdot (\boldsymbol{E} + \boldsymbol{u}_n \times \boldsymbol{B})^2 \tag{5}$$

where σ_P is the Pedersen conductivity, $\boldsymbol{E}$ is the electric field vector, $\boldsymbol{u}_n$ is the neutral wind velocity vector, and $\boldsymbol{B}$ is the magnetic field vector. The dependence of Joule heating on the neutral wind is introduced here because the electric current that results in this heating is passing through the moving neutral gas in a way that the electric field of consequence to heating will depend on its vector in relation with that moving media. Joule heating is deposited to the neutrals either directly or indirectly through the heating of the ions and the subsequent energy exchange between the ions and neutrals, due to their difference in temperature. Due to the limited spatial resolution of Global Circulation Models such as TIE-GCM and GITM, only large-scale electric field structures are captured. On the other hand, it is known that sub-grid small scale electric field structures have a very significant impact to the amount of Joule heating, especially during geomagnetic storms (see, e.g. Matsuo and Richmond (2008)). To account for this, in TIE-GCM, the Joule heating rate, deposited to the neutrals, is multiplied by default by a factor of 1.5. However, as discussed in, e.g., Baloukidis et al. (2023), there are still many unknowns concerning the value that should be used as a function of altitude, solar activity and magnetic local time, leading to large discrepancies between models. These discrepancies and their potential sources have been explored in further detail in Tourgaidis et al. (2025a).

3.1.2 Energetic Precipitating Electrons

Energetic electron precipitation is another heating source in the LTI. Together with heating, energetic particle precipitation passing through the LTI has profound effects on conductivity within this region, and significantly influences chemistry at altitudes below. Electron precipitation also contributes significantly to the observed electron density in the LTI (Verronen et al. (2015)). Within the LTI, energetic precipitating electrons mainly ionize the neutral particles, and this heats the electrons as the newly created electrons (photoelectrons) get thermalized. It is known through simulations that precipitating electrons with energies greater than ~ 200 keV deposit their energy below the D-region ionosphere, at altitudes below ~ 70 km, altering the chemistry of the neutral atmosphere and contributing to ozone destruction through the production of HO_x and NO_x. Precipitating electrons with energies of the order of 10 to 100 keV deposit their energy within the D and E region, at altitudes of approximately 70 to 120 km (e.g., Fang et al. (2008); Turunen et al. (2009); Miyoshi et al. (2010)); Tesema et al. (2020)), altering the chemical and electrical properties of the region and contributing to changes in conductivity and heating. Electrons of energies on the order of or below 1 keV deposit energy to the F region, causing electron density variations. A smaller fraction of the precipitating particle energy flows directly to the neutral gas, particularly via proton precipitation. However, due to a lack of detailed measurements of energetic proton precipitation, this energy fraction is not fully quantified. Electrons above energies of 10 keV provide a significant energy input into the LTI, while electrons above energies of 50 keV can have significant consequences in the chemical composition of the LTI and below, as they ionize neutrals in a series of chemical

https://doi.org/10.5194/egusphere-2025-4315
Preprint. Discussion started: 17 September 2025

reactions that result in the production of H, OH and HO_2, which are termed collectively odd hydrogen, or HO_x, and N, NO and NO_2, which are termed collectively odd nitrogen, or NO_x; These are known to subsequently lead to the catalytic destruction of ozone (Randall et al. (2007).

Electron precipitation is typically caused by a variety of wave-particle interaction mechanisms (e.g., Chorus, Hiss, EMIC etc), which are well modeled and understood theoretically, albeit with significant quantitative uncertainties. These mechanisms have been well described theoretically and have been modeled in detailed wave-particle interaction codes (see, e.g., the comprehensive wave–particle interaction tool-set of models, in Tourgaidis and Sarris (2022), and references therein). Also, the effects of Energetic Precipitating Electrons have been implemented in chemistry-climate models that extend from the surface up to LTI altitudes (see, e.g., Verronen et al. (2016)). However, there are still significant open questions regarding the impacts of EPP. For example, the formation rates of the various NO_x species that are attributed to energetic particle precipitation are currently not known. Furthermore, the coupling between chemical changes, atmospheric heating and cooling rates, and atmospheric dynamics is still an open question (Sinnhuber et al. (2012)). Related to the energy balance and energy deposition in the LTI, a key open question is related to the thermal efficiency of the EPP heating. This is still an open question, as the collision cross-section of precipitating electrons with neutral species is energy dependent. This means that higher energy particles will have smaller collision cross-sections with the neutrals. Thus, higher energy particles are able to penetrate deeper into the atmosphere. At lower altitudes, inelastic collisions become significant, and the kinetic energy of the electrons is converted to thermal energy with higher efficiency. This thermal efficiency is known to be dependent on the particle kinetic energy and thus on altitude dependent in the LTI, but it is poorly known.

3.1.3 Energetic Precipitating Protons

Energetic proton precipitation is caused either by adiabatic loss when ions are transported toward Earth and experience widened loss cones, by the resonant interactions with EMIC waves, or by pitch angle diffusion due to increased field-line curvature radius. Energetic Precipitating Protons can be a significant source of heating of the neutrals in the LTI. Protons in the keV energy range deposit most of their energy in the E region, at altitudes between 100 and 160 km, whereas MeV proton energy deposition occurs at lower altitudes, typically in the D region and below (Galand (2001). They impact the neutrals directly, and can be more significant at certain locations and times, such as the equatorial edge of the evening auroral oval (Galand et al. (2001)). Energetic proton precipitation is generally considered to play a secondary role in affecting the LTI compared to energetic electron precipitation, since the ions usually carry lower energy flux and contribute less to the ionization of the upper atmosphere. This is due to the larger mass and shorter mean free path of protons in the lower thermosphere. Nevertheless, it has been found that, at times, proton precipitation can dominate over electrons in some regions, such as the dusk sector, if electrons do not drift far enough. Furthermore, studies have shown that medium-energy (10s of kev) precipitating protons can carry more energy flux than electrons (Tian et al. (2020)), providing substantial energy deposition down to the ionosphere. At the same time, proton precipitation can lead to significant enhancements in the conductance (Galand and Richmond (2001); Zou et al. (2014)), and can distort the potential pattern in the LTI (Khazanov et al. (2003)). As a conclusion, although it is secondary to

https://doi.org/10.5194/egusphere-2025-4315
Preprint. Discussion started: 17 September 2025

the electron precipitation, the proton precipitation is still important (Newell et al. (2009)), and can not be ignored. At times, proton precipitation can be the major energy source, and thus the primary contributor to auroral emission.

3.1.4 Solar Radiation Heating

During quiet solar and geomagnetic conditions, solar UV Radiation is the most significant heating energy source in the LTI, leading to a significant increase in neutral temperatures in the thermosphere. In particular, solar extreme ultraviolet radiation, EUV and soft X rays are absorbed at altitudes above 90 km and lead to the ionization of the major LTI neutral species, N_2, O, and O_2, and to the creation of the ionosphere. EUV radiation and also leads to the dissociation of the molecular species through direct photo-dissociation and to many indirect processes that driven by ionization, the most important of which is the generation of energetic electrons. These electrons carry the excess energy that is transferred by photoionization, and lead to further ionization, dissociation, and excitation of the neutral constituents, and to a chain of elastic and inelastic processes that transfer the EUV radiation energy into the thermosphere and ionosphere.

Electrons are also heated by ionizing UV radiation. The resulting thermal energy is transferred from electrons to neutrals and ions. UV radiation is the strongest heating source in a global scale. By measuring the ratio of T_e/T_n, which is driven by EPP and UV radiation, it is possible to estimate the fraction of UV radiation that is deposited to the electrons and neutrals. However, it is noted that, similarly to T_i and T_n, co-temporal and co-spatial measurements of T_e and T_n are extremely rare.

There are several missions that have been providing long-term, high-resolution spectral irradiance measurements that have been used for calculating the ionization and dissociation rates in the thermosphere, and for providing the inputs for solar irradiance models. These, in turn, are standard inputs for general circulation models of the thermosphere and ionosphere, such as TIE-GCM. However, there are significant uncertainties related to the photoelectrons that are generated by ionization, which lead to further ionization and dissociation of the neutrals in the thermosphere. Furthermore, the deposition of solar EUV energy in the thermosphere is strongly dependent on both wavelength and altitude, peaking in the 100 to 200 km altitude range, and dropping sharply right below (see, e.g., figure 1(b) of Solomon and Qian (2005)).

3.1.5 Transfer of energy between species due to elastic collisions.

In the presence of collisions between the ions, neutrals and electrons, a transfer of energy will occur that will be dependent upon the temperature difference between the species, the collision frequency and the total plasma density. In the LTI, electron temperatures are expected to always be higher than ion temperatures which, in turn, should be higher than neutral temperatures, else $T_e > T_i > T_n$. Thus, the ions are generally cooled by the transfer of heat to the neutral gas when the temperature of the ions, T_i is larger than the temperature of the neutrals, T_n ($T_i > T_n$). Similarly, the electrons are expected to have higher temperatures than the ions, leading to a heat transfer from the electrons to the ions. The ion-neutral heat transfer rate is given by:

$$q_{\Delta T_{in}} = N_i \nu_{in} \frac{m_i}{m_i + m_n} [3k_B(T_i - T_n)] \tag{6}$$

https://doi.org/10.5194/egusphere-2025-4315
Preprint. Discussion started: 17 September 2025

where ν_{in} is the ion-neutral collision frequency. Thus, simultaneous measurements of T_i and T_n together with knowledge of the ion-neutral collision frequency are needed for the estimation of the heat transfer rate from ions to the neutrals and its comparison with Joule heating rates. Such simultaneous measurements of T_i and T_n are extremely rare, and have only been made for a very limited amount of time by the Atmosphere Explorers AE-C and AE-E in the late 70s and early 80s (see, e.g., Figure 11 of ESA-Daedalus-RfA (2020)), leading to large uncertainties and to a lack of a quantitative understanding of the state of thermal equilibrium of the LTI. This has been highlighted by Peterson et al. (2023), who analyzed simultaneous electron, ion and neutral temperature measurements from AE-C below 140 km, together with remote sensing observations over the Millstone Hill Incoherent Scatter Radar, and demonstrated events where the condition $T_e > T_i > T_n$, does not always hold true. They left open the potential of uncertainties in our quantification and understanding of processes in the LTI, highlighting the need for new measurements. The relative temperatures of ions and neutrals were further studied statistically by Pirnaris and Sarris (2023), who showed that there is a significant percentage of times where the condition $T_e > T_i > T_n$ does not hold true, and pointed to the possibility of missing physics and quantitative understanding in the LTI. In TIE-GCM code, the $T_i \geq T_n$ condition is imposed and is always true.

Similarly to the ion-neutral heating rate, the electron-ion heating transfer rate due to electron-ion collisions is calculated according to:

$$q_{\Delta T_{ei}} = N_e \nu_{ei} \frac{m_e}{m_e + m_i} [3k_B(T_e - T_i)] \tag{7}$$

where ν_{ei} is the electron-ion collision frequency. Finally, the electron-neutral heat transfer rate is given by:

$$q_{\Delta T_{en}} = N_e \nu_{en} \frac{m_e}{m_e + m_n} [3k_B(T_e - T_n)] \tag{8}$$

where ν_{en} is the electron-neutral collision frequency. In general, whereas the heat transfer rates between ions and neutrals are expected to be significant, in particular during active times, the heat transfer rates between ions and electrons and also between electrons and neutrals are much smaller, as will be demonstrated below through simulation.

3.1.6 Radiative cooling

Radiative cooling in the LTI is driven by the emission of infrared radiation from molecules, the most significant of which in terms of radiative cooling are CO_2 and NO. The radiative cooling due to these species plays a crucial role in regulating the temperature and energy balance of the upper atmosphere, especially during geomagnetic disturbances. CO_2 cooling, at 15 μm, is a significant contributor to radiative cooling particularly between 40 and 120 km. NO cooling, at 5.3 μm, on the other hand, becomes the dominant radiative cooler above 120 km, especially during geomagnetic storms and auroral events. This is the altitude where Joule heating is expected to maximize, based on Global Circulation Model results and Incoherent Scatter Radar measurements (see, e.g., Baloukidis et al. (2023)). Thus, even though NO is a relatively minor constituent of the thermosphere compared to other species, it plays a very important role in regulating the energy budget of the thermosphere (see, e.g., Mlynczak et al. (2005); Roble (1995)). Other molecules, such as $O(^3P)$, play a smaller role in radiative cooling; however in the results presented below only the two main radiative cooling terms, NO and CO_2, are included and are presented below.

https://doi.org/10.5194/egusphere-2025-4315
Preprint. Discussion started: 17 September 2025

3.1.7 Heat conduction and Heat Advection

The neutral heat conduction is a significant factor in the determination of neutral temperature, transferring energy between the LTI and the atmosphere below. Heat conduction to the middle atmosphere is the main mechanism of how the Thermosphere gets cooled. In TIE-GCM, the Global Scale Wave Model (GSWM) is used as a lower boundary model. GSWM is a numerical model of planetary waves and solar tides in the Earth's atmosphere from 0 - 125 km (Hagan et al., 1997). However, heat conduction is not explicitly calculated and is not presented in the results below.

In the LTI region, heat advection refers to the transfer of thermal energy by the movement of the neutral species. Heat advection plays a significant role in temperature variations within the LTI, particularly during geomagnetic storms. Vertical heat advection, driven by changes in vertical winds, is a dominant heating process particularly at middle latitudes. Horizontal advection arises from the effects of horizontal winds blowing relatively cold or warm air up and down temperature gradients. Calculations by Killeen et al. (1997) have shown that this term is of secondary importance, playing a role near the summer aurora1 oval, where the strong winds associated with the neutral wind pattern alternately heat and cool the thermosphere, depending on the direction of the local temperature gradients produced by Joule heating. Similarly to heat conduction, heat advection is also not calculated and is not presented below.

3.1.8 Electron cooling from inelastic collisions

In the LTI, both elastic and inelastic collisions are the dominant contributors to the cooling processes of the electron population. During elastic collisions of the electrons with ions and neutrals, as described above in **Equations 7** and **8**, respectively, the kinetic energy of the involved particles is conserved, while that does not hold true in the case of inelastic collisions. Inelastic collisions of electrons with molecules can lead to rotational and vibrational excitations of the involved molecules and consequently to the loss of energy and thus the cooling of the electrons. In TIE-GCM only the vibrational and rotational excitation of the N_2 and O_2 molecules are considered. In addition to the excitation of molecules, two more excitation mechanisms that involve atomic oxygen are expected to be important cooling procedures for the electrons. These are the fine structure excitation of atomic oxygen and the excitation of atomic oxygen to its lowest electronic state ^1D. The relative importance of the different electron cooling mechanisms is a function of the LTI conditions, and especially the neutral and electron temperatures and densities (see e.g. Figure 9.17 in Schunk and Nagy (2009)). In TIE-GCM, the electron cooling is calculated according to equation:

$$L_e = \sum_k [L_{e-vib}(k) + L_{e-rot}(k)] + L_{e-fs}(O) \tag{9}$$

where L_{e-vib} and L_{e-rot} is the cooling due to vibrational and rotational excitation respectively and $L_{e-fs}(O)$ is the cooling due to the fine structure excitation of atomic oxygen and $k = N_2, O_2$. The relevant formulas as used in TIE-GCM can be found in Schunk and Nagy (2009).

https://doi.org/10.5194/egusphere-2025-4315
Preprint. Discussion started: 17 September 2025

3.1.9 Molecular Diffusion, Horizontal Diffusion and Eddy Diffusion

Diffusive processes play a key role in shaping the thermosphere, as they are sufficiently strong to lead to the gravitational separation of the different neutral species (Schunk and Nagy (2009)). Diffusion processes for the ions are also influenced by the by the Earth's magnetic field. At the heat of the significance of diffusion in this region is their collisional nature, since collisions lead to the diffusion of plasma from low density to high density regions and to thermal diffusion. In the diffusion approximation that is followed in TIE-GCM, wave phenomena are not considered; furthermore, the flow is considered to be subsonic. Finally, the ions and electrons are assumed to move together, under the conditions of charge neutrality and charge conservation without electrical currents, a condition that is termed ambipolar diffusion.

Eddy diffusion, also known as turbulent diffusion, is stronger particularly in the lower domain of the thermosphere, up to 105 km altitude, where the various atomic and molecular species are thoroughly mixed. It is driven by turbulent mixing, primarily from the breaking of gravity waves and other instabilities. As altitude increases, molecular diffusion becomes increasingly more important and leads to the diffusive separation between the various neutral species. This diffusive separation region extends from about 110 to 500 km (Schunk and Nagy (2009)), where also most of the ionosphere and thermosphere interactions occur. Turbulent mixing is parameterized by a diffusion coefficient, known as the Eddy diffusion coefficent, which is termed as Kzz in TIE-GCM. Even though it is not well known quantitatively in the thermosphere, it is believed to play a crucial role in the transport of neutral constituents like atomic oxygen and in shaping the composition and temperature profiles of the thermosphere. In TIE-GCM, Eddy diffusion can be set to be day-of-year dependent, or pressure-dependent. The resulting hemispherically-integrated cooling or heating due to Eddy diffusion is relatively small, since it is stronger primarily in the lower boundary of the thermosphere and closer to the turbopause; thus it is not included in the calculations presented herein.

3.2 Thermodynamic equations in TIEGCM

3.2.1 Neutral thermodynamic equation

Thermodynamic calculations for estimating the neutral temperature in TIEGCM are performed by solving the thermodynamic equation for the neutrals, which includes a number of heating and/or cooling terms. The heating terms, Q_tot, include: Joule heating, solar radiation heating (EUV, Schuman-Runge bands and continuum), heating due to ion chemistry, heating generated by the recombination of the atomic oxygen (O_2) in the lower thermosphere, heating due to molecular diffusion, photoelectron heating, horizontal diffusion, heating due to electron-neutral collisions, heat transfer by vertical molecular heat conduction, adiabatic heating/cooling due to eddy diffusion, heat transfer due to vertical advection, adiabatic heating and cooling by the vertical neutral winds. Cooling terms, L_tot, include CO_2 cooling, NO cooling and $O(^3P)$ cooling. In TIE-GCM the thermodynamic equation for the neutral species is given as:

$$\frac{\partial T_n}{\partial t} = \overbrace{\frac{ge^z}{p_0 C_p}\frac{\partial}{\partial Z}\left[\frac{K_T}{H}\frac{\partial T_n}{\partial Z} + K_E H^2 C_p \rho\left(\frac{g}{C_p} + \frac{\partial T_n}{H\,\partial Z}\right)\right]}^{\text{Heat transfer by vertical molecular conduction and adiabatic heating/cooling by eddy diffusion}} - \overbrace{\boldsymbol{v_n}\cdot\nabla T_n}^{\text{Heat transfer due to horizontal advection}} - \overbrace{w\left(\frac{\partial T_n}{\partial Z} + \frac{R^* T_n}{C_p \overline{m}}\right)}^{\text{Adiabatic heating and cooling due to vertical winds}} + \overbrace{Q_{tot} - L_{tot}}^{\text{Other heating and cooling terms}} \quad (10)$$

https://doi.org/10.5194/egusphere-2025-4315
Preprint. Discussion started: 17 September 2025

where g is the gravitational acceleration, C_p is the specific heat, p_0 is the TIE-GCM reference pressure, K_T is the thermal conductivity, H is the scale height, K_E is the eddy diffusion coefficient, ρ is the neutral density, $\boldsymbol{v}_n$ is the horizontal neutral velocity, W is the vertical neutral velocity, R^* is the gas constant, $\overline{m}$ is the mean mass of the neutral species, Q_{tot} are the heating terms and L_{tot} are the cooling terms as mentioned in the previous paragraph. In this paper we will not include in our calculations the contributions from the heat conduction, the eddy diffusion, the horizontal advection and the contributions of vertical winds. It is noted that, according to the TIE-GCM manual, the total heating,Q_{tot}, does not explicitly calculate the energy transfer from the ions to the neutrals, as shown in Figure 2. Instead, it assumes that eventually all Joule heating (i.e., the Joule heating that is directly deposited to the neutrals and the Joule heating that is deposited to the ions) will eventually go to the neutrals. This is due to the fact that, eventually, all Joule heating is thermal energy deposited to the neutrals (and partially radiated away again). To facilitate the discussion of the ion thermodynamics we employ the following conceptual model: Ions and neutrals are forced to convect relative to each other by the magnetospheric electric field and neutral inertia. Collisions between both randomize/thermalize their relative motion. Because the density of neutrals is much larger than of ions (factor 1000 in the F region, 10000-100000 in the E region), a single neutral will collide relatively rarely with an ion, with a collision time that is, on average, $1/\nu_{in} * n_n/N_e$, while an ion collision time is $1/\nu_{in}$. By further neutral-neutral collisions, the collided neutrals transfer their gained thermal energy to all other neutrals, while the collided ions do not have this opportunity. This explains the aforementioned $T_i > T_n$. The ions transfer their thermal energy to cooler neutrals in further ion-neutral collisions. This justifies to split the Joule heating effect on the ions into two terms: $Q_J^{T_n}$, that goes directly to the neutrals and $Q_J^{T_i}$, that initially heats the ions and eventually is deposited to the neutrals via the $q_{\Delta T_{in}}$ term, as calculated by Equation 6, and as further discussed below.

3.2.2 Ion thermodynamic equation

From the point of view of the ions, the heating rates include a fraction of the Joule heating and heating due to elastic collisions with electrons. On the other hand, ions are cooled due to ion-neutral collisions. Regarding the Joule heating, only a part of the total Joule heating is directly deposited to the ions, given (in TIEGCM) as:

$$Q_J^{T_i} = \frac{\overline{m_n}}{\overline{m_n} + \overline{m_i}} Q_J \tag{11}$$

where $Q_J^{T_i}$ is the part of the Joule heating directly deposited to the ions, Q_J is the total Joule heating, $\overline{m_n}$ and $\overline{m_i}$ are the mean molecular weights of the neutral and the ion species respectively. Thus the thermodynamic equation for the ions is given as:

$$Q_{ie} + Q_J^{T_i} = L_{in} \tag{12}$$

where Q_{ie} is the heating of ions due to ion-electron collisions and L_{in} is the cooling of the ions due to ion-neutral collisions. In general, the contributions of the ion-electron collisions Q_{ie} are negligible small, thus the part of the Joule heating deposited to the ions $Q_J^{T_i}$, goes eventually to the neutrals through ion-neutral interactions (L_{in}).

https://doi.org/10.5194/egusphere-2025-4315
Preprint. Discussion started: 17 September 2025

3.2.3 Electron thermodynamic equation

For the estimation of the electron temperature, TIEGCM assumes a quasi-steady state and neglects heating due to horizontal gradients of the electron temperature and density, due to the thermaelectric heat flux, and due to the adiabatic expansion and heat advection. The heating rates for the electrons, include solar EUV, Joule heating contributions, deactivation of excited neutral and ion species, dissociative recombination of electrons and ions and energetic particle precipitation. In TIEGCM calculations, only the solar EUV and the energetic particle precipitation are considered as heating sources as the contributions from the rest of the mechanisms are negligibly small. Regarding the cooling of the electrons, the calculations include cooling due to elastic collisions with neutrals (O, O_2, N_2), to vibrational excitation of N_2 and O_2, to rotational excitation of N_2 and O_2, and to the fine structure excitation of O.

$$\overbrace{\sin^2 I \frac{\partial}{H\partial Z}\left(K^e \frac{\partial T_e}{H\partial Z}\right)}^{\text{Heat transfer due to conduction parallel to the geomagnetic field}} + \overbrace{\sum Q_e}^{\text{Heating due to solar UV radiation and EPP}} = \overbrace{\sum L_e}^{\text{Cooling due to elastic and inelastic collisions with neutrals and ion-electron collisions}} \tag{13}$$

where I is the geomagnetic dip angle and K^e is the electron thermal conductivity parallel to the geomagnetic field. In our calculations, only the heating due to solar EUV and EPP and the cooling terms are considered.

4 Results

The energy flow terms that are shown in **Figure 2** were calculated at every grid point of the TIE-GCM, and were subsequently hemispherically integrated, to provide the total absolute value of each heating term. In the following figures results for the north hemisphere are presented. These are shown below for two time instances of the St Patrick's day storm of March 2025: at the peak of the storm, as indicated by the lowest value of the D_{st} index, and 24 hours before the peak of the storm. The later time is selected so as to remove diurnal effects from the estimates, and to provide a pre-storm value that can be reasonably compared to the storm-time values. In the following, the energy transfer terms are described in three different perspectives: energy flow according to the heating or cooling of the neutrals, according to the ions and according to the electrons. Hence, as an example, energy that is transferred from, e.g., the ions to the neutrals would be considered a cooling term for the ions, but a heating term for the neutrals. In the corresponding diagrams of Figures 3, 4, and 5, energy that is transferred from a species (i.e. acting as a cooling mechanism of the respective species) is marked with an outward blue arrow. Energy that is added to the species is marked with an inward-pointing, red arrow. A curved/wavy line and arrow indicate a radiative transfer process, whereas a dashed line marks a process that is not calculated in TIE-GCM or that is not included in our discussion due to comparatively very low values. Next to each diagram, the bar plots show the corresponding calculations of the various terms before the storm (left) and at the peak of the storm (right). The blue bars correspond to calculations that were performed using the Weimer-2005 model as driver of TIE-GCM, whereas the orange bars correspond to calculations that were performed using the AMIE model.

https://doi.org/10.5194/egusphere-2025-4315
Preprint. Discussion started: 17 September 2025

4.1 Energy Flow According to the Neutrals

The energy flow from and to the neutral species of the LTI is shown in the left panel of **Figure 3**. As shown in this diagram, the neutrals are heated directly by EUV radiation, by Joule heating due to the differential velocity between the neutral winds and the ions under the effects of electric fields, by collisional interactions with the ions due to their differences in temperatures, by elastic collisions with electrons, by inelastic collisions with electrons, and by Energetic Precipitating Protons. The neutral species are cooled by heat conduction to the middle atmosphere, by horizontal and vertical heat advection, and by radiative cooling. The main radiative cooling elements in the LTI are CO_2 and NO. In principle, N_2 and O_2 also participate in IR radiation, however they are not included in TIE-GCM, and their radiative cooling effects are not included herein.

In the following, the energy sources and energy flow terms that are discussed in the left panel of **Figure 3** are calculated numerically based on TIE-GCM. In the middle and right panels of **Figure 3**, two snapshots are plotted, corresponding to a quiet-time instance and to the peak of the storm. A movie of the evolution of these terms is included as **Supplementary Material S1**. As discussed above, the peak of St. Patrick's day storm is defined by the time of minimum Dst and minimum $SYM-H$ indices, which was on March 17, 2015, at 23:30. To illustrate the quiet-time energy energy sources and energy flow terms, a time instance one day before the peak of the storm is selected. Thus, the middle panel of **Figure 3** shows the quantification of the heating and cooling terms one day before the peak of St. Patrick's day storm, on March 16, 2015, at 23:30. This time is marked in Figure 1with a blue dashed vertical line. At this time, small discrepancies can be seen in the two different estimates of Joule heating and the heating from the ions that are based on the different TIE-GCM runs with the two different external driving models, with the estimates that are based on the AMIE model showing larger amounts of heating compared to the Weimer model. As it is shown, the part of the Joule heating directly deposited to the neutrals and the $q\Delta T_{in}$ i.e. the heating of the neutrals due to collisions with the ions are almost equal, meaning that in quiet times half of the total Joule heating is directly deposited to the neutrals and the other half goes directly to the ions and finally to the neutrals through ion-neutral collisions. Elastic and inelastic collisions with electrons are of little impact to the neutrals. The largest heating source during this time is the heating due to EUV and EPP heating followed by the heating due to the recombination of O_2. Radiative cooling by CO_2 is the largest cooling term, followed by the radiative cooling by NO. The least important heating terms are the heating due to the molecular diffusion, the horizontal diffusion and due to photoelectrons.

The right panel of **Figure 3** shows the quantification of the heating and cooling terms during the peak of St. Patrick's day storm, on March 17, 2015, at 23:30. This time is marked in **Figure 1**with a red dashed vertical line. In the right panel of **Figure 3**, it is noted that Joule heating directly deposited to the neutrals exceeds the heating deposited to the neutrals from the ions, which corresponds to the $q\Delta_T in$ term. Comparing the two different driving models, it is noted that the Weimer model gives lower estimates of Joule heating than the AMIE model. This, as discussed below, is attributed to the inclusion of smaller scales in the AMIE model, enabled by the long-term assimilation of multiple datasets. The heating due to EUV and EPP is only slightly elevated compared to the corresponding quiet time EUV and EPP heating. All the other heating terms, even though small compared to Joule heating and ion heating, are significantly increased with the exception of the heating due to horizontal diffusion. Regarding the cooling terms, it can be seen that CO_2 is a stronger cooling agent in the pre-storm

https://doi.org/10.5194/egusphere-2025-4315
Preprint. Discussion started: 17 September 2025

time, whereas NO cooling is drastically increased post-storm, greatly exceeding CO_2 cooling. This has been reported in past studies, who have pointed out that during quiet times radiation in the IR is the dominant thermospheric cooling agent (see, e.g., Mlynczak et al. (2014)), whereas cooling due to NO emission is greatly enhanced during storms, and is considered as a "natural thermostat" that contributes to the recovery of the thermosphere from the temperature increases due to Joule heating during solar geomagnetic storms, typically within 2-3 days (see, e.g., Mlynczak et al. (2003), Mlynczak et al. (2005)).

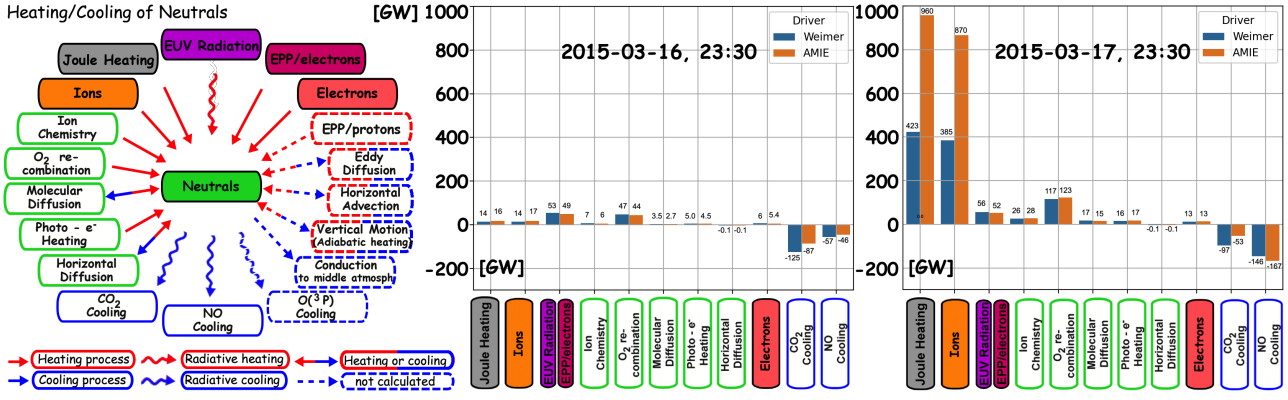

Figure 3. Left: Overview of the main energy sources and energy flow to and from the neutrals in the Lower Thermosphere - Ionosphere. Terms in solid arrows and boxes are estimated through TIE-GCM, whereas terms in dashed arrows and boxes are not calculated. Right (Middle): Quantification of the main energy terms at the peak of (one day before the peak of) St. Patrick's day storm. Two electric potential drivers are used, according to the Weimer 2005 and the AMIE models, as marked.

4.2 Energy Flow According to the Ions

The energy flow from and to the ion species of the LTI is shown schematically in **Figure 4**. Thus, the ions are heated directly by Joule heating, due to the differential velocity between the neutral winds and ion drifts under the effects of electric fields. Ions also exchange energy with the electrons due to their differences in temperature, via electron-ion elastic collisions, that are dependent on the difference in temperatures between the electrons and the ions, according to **Equation 7**. Finally, ions heat the neutral species via ion-neutral collisional interactions, due to their differences in temperatures, as discussed above and calculated via **Equation 6**. A movie of the evolution of these terms is included as **Supplementary Material S2**. In the middle panel of **Figure 4**, corresponding to quiet-time conditions, we can see that, before the peak of the storm, Joule heating is the most significant heating source of the ions, and that the heating from the electrons is a small fraction of the Joule heating. The total heating of the ions is transferred to the neutrals, which is considered a cooling term for the ions. In the right panel we can see that, during the peak of the storm, both the heating of the ions due to Joule heating and their cooling via heat transfer to the neutrals are largely increased.

https://doi.org/10.5194/egusphere-2025-4315
Preprint. Discussion started: 17 September 2025

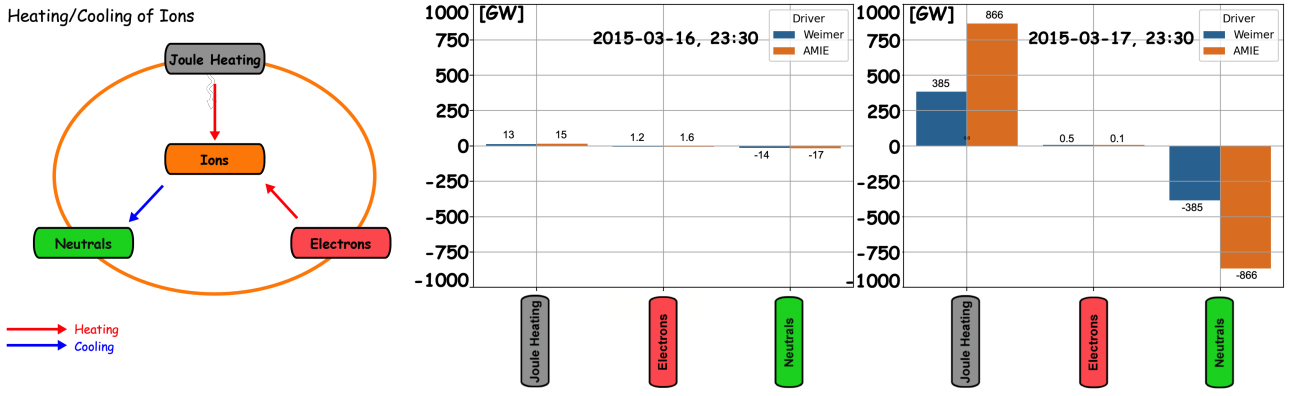

Figure 4. Left: Overview of the main energy sources and energy flow to and from the Ions in the Lower Thermosphere - Ionosphere. Terms in red arrows correspond to heating of the ions whereas terms in blue arrows correspond to cooling of the ions. Right (Middle): Quantification of the main energy terms at the peak of (one day before the peak of) St. Patrick's day storm. Two electric potential drivers are used, according to the models by Weimer 2005 and AMIE, as marked.

4.3 Energy Flow According to Electrons

The heating sources of electrons generally include solar EUV radiation, heating from electron precipitation, Joule heating, as well as heating from the deactivation of excited neutral and ion species and from the dissociative recombination of electrons with ions. On the other hand, electrons are cooled via electron-neutral elastic and inelastic collisions, as described in Equations 8 and 9 respectively (see Chapter 9.7 of Schunk and Nagy (2009)). Electrons are also cooled via collisions with the ions due to their temperature difference, as described in Equation 7, as they are generally considered to be hotter than ions. Finally, electrons are also cooled by conduction. In TIE-GCM, only solar EUV radiation and energetic particle precipitation are considered as heating terms, while all other heating contributions are considered to be small and are neglected. As cooling terms, the energy transfer to the neutrals and ions is calculated. Furthermore, in TIE-GCM, a quasi-steady state is assumed for the electrons, and thus the thermal electric heat flux, horizontal gradients of electron temperature, T_e, and electron density, N_e, as well as adiabatic expansion and heat advection, are ignored. The heating and cooling sources of the electrons that are considered in the calculations herein are summarized schematically in the left panel of **Figure 5**. The electron thermal conduction to lower altitudes, along their propagation parallel to the magnetic field, is not calculated herein; this is marked in a dashed blue box. The heating and cooling terms according to the electrons are presented quantitatively in the middle and right panels of **Figure 5**, as above, whereas their time evolution is shown as a movie in **Supplementary Material S3**. Both before and after the storm, there are very small differences between the heating and cooling rates between the Weimer 2005 and the AMIE model runs. Regarding the cooling rates, the differences of the cooling to the neutrals due to elastic collisions, and the cooling to the ions are very small. On the other hand the heat loss to the neutrals due to inelastic collisions become large during the peak of the storm, following the pattern of the EUV/EPP heating. From the above, we can infer that during the peak of the storm the

https://doi.org/10.5194/egusphere-2025-4315
Preprint. Discussion started: 17 September 2025

heating of the electrons is increased mostly due to enhanced EPP, and the cooling of the electrons is mainly controlled through the inelastic collisions with the neutrals.

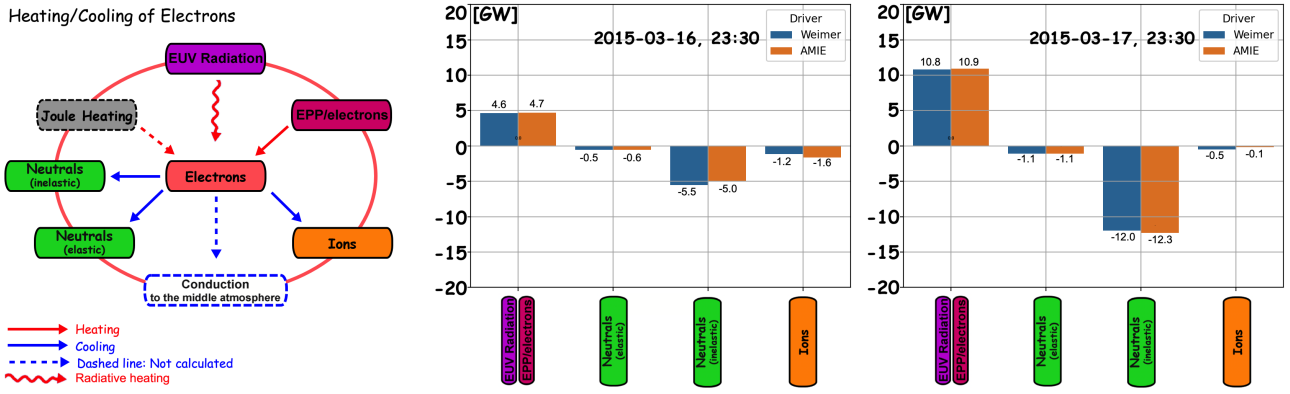

Figure 5. Left: Overview of the main energy sources and energy flow to and from the Electrons in the Lower Thermosphere - Ionosphere. Terms in red arrows correspond to heating of the ions whereas terms in blue arrows correspond to cooling of the ions. Right (Middle): Quantification of the main energy terms at the peak of (one day before the peak of) St. Patrick's day storm. Three electric potential drivers are used, according to the models by Weimer, Heelis, and AMIE, as marked.

5 Discussion

Despite the comprehensive understanding of the basic framework that is presented in **Figure 2** and is demonstrated in the above calculations, there are significant gaps in the quantification of some of the key energy sources and processes processes, most notably Joule heating and the associated transfer of energy from the ions to the neutrals. This is primarily due to severe limitations in available data sets. It is noted, for example, that the entire available dataset of simultaneous ion, neutral and electron temperature measurements in the LTI at 100 to 200 km consists of only 60 hours of observations (see, e.g., Figure 11 of ESA-Daedalus-RfA (2020)), with the majority of measurements originating from the Atmosphere Explorer C and E satellites of the 1970s. Due to the lack of comprehensive measurements, the actual amount of Joule heating, the most important heating source in the LTI, varies greatly between estimation methodologies and input models. This has also been discussed and demonstrated in a study by Baloukidis et al. (2023), who compared Joule heating estimates from TIE-GCM and those derived from European Incoherent Scatter Scientific Association (EISCAT) radar measurements. That study found that TIE-GCM tends to overestimate Joule heating for low geomagnetic activity but underestimate them for high geomagnetic activity compared to EISCAT, and highlighted the need to account for small-scale effects in TIE-GCM. This has also been demonstrated by Tourgaidis et al. (2025a), who performed four different GCM simulations using TIE-GCM and GITM under two different electric potential models as external drivers, and compared the results against empirical model estimates. That study found that there are significant discrepancies between the GCMs, and even larger differences between GCMs and empirical models, that require new measurements and a revisit to the Joule heating estimates in the LTI.

https://doi.org/10.5194/egusphere-2025-4315
Preprint. Discussion started: 17 September 2025

Due to the lack of comprehensive co-located, co-temporal measurements, it is possible that even basic principles of the state of thermal equilibrium need to be revisited. For example, as recent re-analyses of the AE dataset by Peterson et al. (2023) and Pirnaris and Sarris (2023) has shown, there are times where the temperatures of the neutrals, T_n, are higher than the temperatures of the ions, T_i, reversing the commonly accepted condition that $T_i > T_n$, which is enforced in current empirical models of the LTI, such as IRI-2020 (Bilitza et al. (2022)) and NRLMSIS 2.0 (Emmert et al. (2021)); this condition is also enforced in TIE-GCM v2.0. This leads to insufficient knowledge in understanding the effects of the external drivers to the overall energy budget and to the state variables of the LTI.

In comparing the various heating terms in **Figures 3**, **4** and **5**, it can be seen that during the pre-storm time the heating due to EUV/EPP and the recombination of O_2 are the largest heating terms. During the peak of the storm, Joule heating and ion-neutral heating become the main heating sources by far, followed by the heating due to the recombination of O_2, whereas the heating due to the EUV/EPP is only slightly increased during the storm. Regarding the cooling of the neutrals, it can be seen that before the storm, the main cooling term is the CO_2 cooling, while at the peak of storm the NO cooling becomes larger for both the AMIE and Weimer 2005 runs, although significant discepancies can be seen in their estimates.

With respect to the differences in the estimates of Joule heating between the Weimer 2005 and the AMIE models, it is noted that one crucial difference between the two model runs is the spatial scales that can be resolved by each. The Weimer-2005 empirical model has a resolution of $\sim 2-3^o$ in magnetic latitude and ~ 1 in MLT. On the other hand, the AMIE assimilative model is in general finer than empirical models, but is highly dependent on available data density. Typically, the AMIE model can achieve a resolution of $\sim 1-2^o$ in magnetic latitude and $\sim 15-30$ minutes in MLT. On the other hand, the grid resolution of TIE-GCM is 2.5×2.5 degrees in latitude and longitude. Thus, due to its coarse spatial resolution, TIE-GCM cannot resolve small-scale (sub-grid) electric field variability. In reality though, the small-scale electric field variability can greatly enhance Joule heating due to its quadratic dependence on the electric field ($Q_j = \Sigma_P E^2$); thus an underestimation of Joule heating is expected in the model, if sub-grid variability is not well represented. To partially compensate this, TIE-GCM employs an empirical Joule heating enhancement factor, termed $Joulefac$, which scales the modeled heating to account for unresolved small-scale structures. This approach provides a climatologically reasonable estimate of total heating but may underestimate localized responses during disturbed conditions. Moreover, the use of higher resolution electric fields from assimilative techniques instead of empirical models, compensates part of the small-scale variability but nevertheless, residual underestimation persists (i.e. scales below 1^o). As discussed in Baloukidis et al. (2023), using a $Joulefac$ parameter that is dependent on the solar wind parameters is required, but this relies on critically missing measurements in the LTI, where Joule heating maximizes. Another key missing aspect of Joule heating involves the characterization of its altitudinal distribution. Whereas ground-based measurements can provide the altitude profiles of Joule heating, they lack the required resolution, and also do not provide all measurements that are required in the estimation of Joule heating. As demonstrated by Vogt et al. (2023), a twin-spacecraft mission with altitudinal separation and with comprehensive instrumentation that performs measurements in the altitudes of interest would be able to provide the altitude profiles with sufficient statistical significance so as to derive the climatological characterization of Joule heating as a function of altitude, while also resolving the open question of the significance of Joule heating at small scales.

https://doi.org/10.5194/egusphere-2025-4315
Preprint. Discussion started: 17 September 2025

With respect to the differences in the heat exchange rates between ions and neutrals between the two model runs, it is noted that these are proportional to the Joule heating rate estimates, as shown in **Figure 3** and **4**. This is because the heat exchange rates between ions and neutrals via collisional interactions will depend on the corresponding temperatures, T_i and T_n, as shown in Equation 6. Since different Joule heating rates will result in different temperature increases of the ions, a higher Joule heating rate is indeed expected to result in higher ion-neutral heat exchange, as it is observed herein.

In Figure 3, it can be seen that the cooling terms from the main radiative cooling species, NO and CO_2, are also significantly different for the two runs with the different drivers, both before the storm and during the peak of the storm.

It is noted that heat advection and heat conduction are also calculated in TIE-GCM and are a part of the energy budget of the neutrals and plasmas. The heat conduction term depends on gradients in temperature, whereas the heat advection will depend on gradient in the velocity. These terms are calculated at every step in TIE-GCM, but are not included in the presented analysis.

6 Summary and Conclusions

The storage, transport and transformation of energy in the Lower Thermosphere-Ionosphere (LTI) was studied via model runs using NCAR's TIE-GCM in order to estimate energy sources and sinks, energy transfer rates and the energy partitioning between the different species. The model runs were performed for the 2015 St. Patrick's day geomagnetic super-storm, for the period 15-21 March. To explore the variability in the quantification of the energy budget and energy flow, we performed estimates from two different simulations of TIE-GCM, using two different high latitude potential models as external drivers: one empirical model, Weimer 2005, and one assimilative model, AMIE. The resulting energy budget and the corresponding partitioning of energy between species were inter-compared between the two runs, before and after the storm. These two runs allow to explore the range of variability of various heating and cooling terms under the effect of the largely unknown high-latitude electric potential. We then quantified the variability of the main energy flow estimates from three different perspectives: that of the neutrals, of the ions and of the electrons. It is noted that, whereas in most studies the state of the LTI is presented from the viewpoint of the neutrals, herein a view of the main energy transfer terms is presented separately according to each species.

It was found that the largest differences in the energy flow for the different processes is found primarily in the Joule heating rates, and in the associated heating from the ions to the neutrals. Specifically, it was found that the AMIE model run gives more than twice as large Joule heating and ion-to-neutral heating than the Weimer 2005 model. These discrepancies are attributed to the average electric field that is estimated by each of the model drivers, as higher fields will give higher Joule heating; these discrepancies are also due to the different temporal variability in the electric field and also due to the differences in the small spatial scales of the electric field that can be resolved by each of the models, as higher spatial and temporal variability will result in higher Joule heating. This sub-grid variability of the electric fields is a key unknown factor in LTI electrodynamics and energetics, and has significant implications for the quantification and prediction of the effects of energy inputs such as Joule heating for density enhancements in the LTI and the resulting drag effects on Low Earth Orbit satellites.

https://doi.org/10.5194/egusphere-2025-4315
Preprint. Discussion started: 17 September 2025

Through the model runs it is concluded that obtaining new, systematic measurements of all required parameters for the calculation of Joule heating is required to improve our understanding of the energy balance and energy transfer processes. Obtaining co-located, co-temporal measurements within this region requires placing state-of-the-art instruments on an in situ platform that samples this region along track, providing statistically significant measurements (e.g., Sarris et al. (2023a)). Such mission concepts are actively pursued at ESA and NASA (e.g., Sarris et al. (2020); Pfaff et al. (2022); ESA/NASA-ENLoTIS-Report (2024)). The measurements gathered in this manner will enable estimating the actual Joule heating into the LTI and will reveal how collisions between neutral and charged species affect the energetics of the LTI, providing a critically missing link in the energy budget of the LTI.

Code and data availability.

The datasets used in the study are available at Tourgaidis et al. (2025b).

Video supplement.

The three videos in this supplement show the time-evolution of the various heating and cooling terms during the period of the storm, from March 15, 2015 to March 21, 2015, according to the neutrals, ions and electrons, as marked. The videos can be accessed at Tourgaidis et al. (2025b).

Author contributions. ST, DB and PP performed the TIE-GCM runs. ST, DB, PP worked on the code for the analysis of the results. ST performed the calculations of the various heating terms. TS and ST worked on the preparation of the manuscript. TS, SB and KP contributed to the discussion of the results.

Competing interests. The authors declare that they have no conflict of interest.

Acknowledgements. The authors acknowledge the use of data obtained from [SuperDARN (http://vt.superdarn.org/tiki-index.php), SuperMAG (https://supermag.jhuapl.edu), and AMPERE (http://ampere.jhuapl.edu)] for the period of 15-21 March 2015.

https://doi.org/10.5194/egusphere-2025-4315
Preprint. Discussion started: 17 September 2025

References

Akasofu, S.-I.: Energy coupling between the solar wind and the magnetosphere, Space Science Reviews, 28, 121–190, 1981.

Baloukidis, D., Sarris, T., Tourgaidis, S., Pirnaris, P., Aikio, A., Virtanen, I., Buchert, S., and Papadakis, K.: A comparative assessment of the distribution of Joule heating in altitude as estimated in TIE-GCM and EISCAT over one solar cycle, Journal of Geophysical Research: Space Physics, 128, e2023JA031 526, 2023.

Bilitza, D., Pezzopane, M., Truhlik, V., Altadill, D., Reinisch, B. W., and Pignalberi, A.: The International Reference Ionosphere model: A review and description of an ionospheric benchmark, Reviews of geophysics, 60, e2022RG000 792, 2022.

Codrescu, M., Fuller-Rowell, T., and Foster, J.: On the importance of E-field variability for Joule heating in the high-latitude thermosphere, Geophysical Research Letters - GEOPHYS RES LETT, 22, 2393–2396, https://doi.org/10.1029/95GL01909, 1995.

Dmitriev, A., Suvorova, A., Klimenko, M., Klimenko, V., Ratovsky, K., Rakhmatulin, R., and Parkhomov, V.: Predictable and unpredictable ionospheric disturbances during St. Patrick's Day magnetic storms of 2013 and 2015 and on 8–9 March 2008, Journal of Geophysical Research: Space Physics, 122, 2398–2423, 2017.

Emmert, J. T., Drob, D. P., Picone, J. M., Siskind, D. E., Jones Jr, M., Mlynczak, M. G., Bernath, P. F., Chu, X., Doornbos, E., Funke, B., et al.: NRLMSIS 2.0: A whole-atmosphere empirical model of temperature and neutral species densities, Earth and Space Science, 8, e2020EA001 321, 2021.

ESA-Daedalus-RfA: Earth explorer 10 candidate mission Daedalus report for assessment (RfA), Report for assessment, ESA Available at: https://esamultimedia. esa. int/docs/EarthObservation/EE10_Daedalus_Report-for-Assessment-v1. 0_13Nov2020. pdf(Accessed December 27, 2022), 2020.

ESA/NASA-ENLoTIS-Report: Exploring Earth's Interface with Space – The Scientific Case for a Satellite Mission to the Lower Thermosphere-Ionosphere Transition Region, Tech. Rep. ESA-EOPSM-ELTI-RP-4592 / NASA/CR-20240013551, European Space Agency (ESA), Noordwijk, The Netherlands and National Aeronautics and Space Administration (NASA), Washington DC, United States of America, http://doi.org/10.5270/ESA-NASA.LTI-SC.2024-07-v1.0, 2024.

Fang, X., Randall, C. E., Lummerzheim, D., Solomon, S. C., Mills, M. J., Marsh, D. R., Jackman, C. H., Wang, W., and Lu, G.: Electron impact ionization: A new parameterization for 100 eV to 1 MeV electrons, Journal of Geophysical Research: Space Physics, 113, 2008.

Galand, M.: Introduction to special section: Proton precipitation into the atmosphere, Journal of Geophysical Research: Space Physics, 106, 1–6, 2001.

Galand, M. and Richmond, A. D.: Ionospheric electrical conductances produced by auroral proton precipitation, Journal of Geophysical Research: Space Physics, 106, 117–125, 2001.

Galand, M., Fuller-Rowell, T., and Codrescu, M.: Response of the upper atmosphere to auroral protons, Journal of Geophysical Research: Space Physics, 106, 127–139, 2001.

Goldstein, J., Angelopoulos, V., De Pascuale, S., Funsten, H., Kurth, W., LLera, K., McComas, D., Perez, J., Reeves, G., Spence, H., et al.: Cross-scale observations of the 2015 St. Patrick's day storm: THEMIS, Van Allen Probes, and TWINS, Journal of Geophysical Research: Space Physics, 122, 368–392, 2017.

Hagan, M., Chang, J., and Avery, S.: Global-scale wave model estimates of nonmigrating tidal effects, Journal of Geophysical Research: Atmospheres, 102, 16 439–16 452, 1997.

Heelis, R. and Maute, A.: Challenges to understanding the Earth's ionosphere and thermosphere, Journal of Geophysical Research: Space Physics, 125, e2019JA027 497, 2020.

https://doi.org/10.5194/egusphere-2025-4315
Preprint. Discussion started: 17 September 2025

Heelis, R., Lowell, J. K., and Spiro, R. W.: A model of the high-latitude ionospheric convection pattern, Journal of Geophysical Research: Space Physics, 87, 6339–6345, 1982.

Hudson, M., Jaynes, A., Kress, B., Li, Z., Patel, M., Shen, X.-C., Thaller, S., Wiltberger, M., and Wygant, J.: Simulated prompt acceleration of multi-MeV electrons by the 17 March 2015 interplanetary shock, Journal of Geophysical Research: Space Physics, 122, 10–036, 2017.

Jaynes, A. N., Ali, A., Elkington, S. R., Malaspina, D. M., Baker, D. N., Li, X., Kanekal, S. G., Henderson, M. G., Kletzing, C., and Wygant, J. R.: Fast diffusion of ultrarelativistic electrons in the outer radiation belt: 17 March 2015 storm event, Geophysical Research Letters, 45, 10–874, 2018.

Kan, J. and Lee, L.: Energy coupling function and solar wind-magnetosphere dynamo, Geophysical Research Letters, 6, 577–580, 1979.

Kanekal, S., Baker, D., Fennell, J., Jones, A., Schiller, Q., Richardson, I., Li, X., Turner, D., Califf, S., Claudepierre, S., et al.: Prompt acceleration of magnetospheric electrons to ultrarelativistic energies by the 17 March 2015 interplanetary shock, Journal of Geophysical Research: Space Physics, 121, 7622–7635, 2016.

Khazanov, G., Liemohn, M., Newman, T., Fok, M.-C., and Spiro, R.: Self-consistent magnetosphere-ionosphere coupling: Theoretical studies, Journal of Geophysical Research: Space Physics, 108, 2003.

Killeen, T., Burns, A., Azeem, I., Cochran, S., and Roble, R.: A theoretical analysis of the energy budget in the lower thermosphere, Journal of Atmospheric and Solar-Terrestrial Physics, 59, 675–689, 1997.

Knipp, D., Welliver, T., McHarg, M., Chun, F., Tobiska, W., and Evans, D.: Climatology of extreme upper atmospheric heating events, Advances in Space Research, 36, 2506–2510, 2005.

Lyons, L., Gallardo-Lacourt, B., Zou, S., Weygand, J., Nishimura, Y., Li, W., Gkioulidou, M., Angelopoulos, V., Donovan, E., Ruohoniemi, J., et al.: The 17 March 2013 storm: synergy of observations related to electric field modes and their ionospheric and magnetospheric effects, Journal of Geophysical Research: Space Physics, 121, 10–880, 2016.

Marsal, S., Torta, J., Segarra, A., and Araki, T.: Use of spherical elementary currents to map the polar current systems associated with the geomagnetic sudden commencements on 2013 and 2015 St. Patrick's Day storms, Journal of Geophysical Research: Space Physics, 122, 194–211, 2017.

Matsuo, T. and Richmond, A. D.: Effects of high-latitude ionospheric electric field variability on global thermospheric Joule heating and mechanical energy transfer rate, Journal of Geophysical Research: Space Physics, 113, 2008.

Miyoshi, Y., Katoh, Y., Nishiyama, T., Sakanoi, T., Asamura, K., and Hirahara, M.: Time of flight analysis of pulsating aurora electrons, considering wave-particle interactions with propagating whistler mode waves, Journal of Geophysical Research: Space Physics, 115, 2010.

Mlynczak, M., Martin-Torres, F. J., Russell, J., Beaumont, K., Jacobson, S., Kozyra, J., Lopez-Puertas, M., Funke, B., Mertens, C., Gordley, L., et al.: The natural thermostat of nitric oxide emission at 5.3 μm in the thermosphere observed during the solar storms of April 2002, Geophysical Research Letters, 30, 2003.

Mlynczak, M. G., Martin-Torres, F. J., Crowley, G., Kratz, D. P., Funke, B., Lu, G., Lopez-Puertas, M., Russell III, J. M., Kozyra, J., Mertens, C., et al.: Energy transport in the thermosphere during the solar storms of April 2002, Journal of Geophysical Research: Space Physics, 110, 2005.

Mlynczak, M. G., Hunt, L. A., Mertens, C. J., Thomas Marshall, B., Russell III, J. M., Woods, T., Earl Thompson, R., and Gordley, L. L.: Influence of solar variability on the infrared radiative cooling of the thermosphere from 2002 to 2014, Geophysical Research Letters, 41, 2508–2513, 2014.

https://doi.org/10.5194/egusphere-2025-4315
Preprint. Discussion started: 17 September 2025

Newell, P., Sotirelis, T., Liou, K., Meng, C.-I., and Rich, F.: A nearly universal solar wind-magnetosphere coupling function inferred from 10 magnetospheric state variables, Journal of Geophysical Research: Space Physics, 112, 2007.

Newell, P. T., Liou, K., and Wilson, G. R.: Polar cap particle precipitation and aurora: Review and commentary, Journal of atmospheric and solar-terrestrial physics, 71, 199–215, 2009.

Ozeke, L., Mann, I., Olifer, L., Dufresne, K., Morley, S., Claudepierre, S., Murphy, K., Spence, H., Baker, D., and Degeling, A.: Rapid outer radiation belt flux dropouts and fast acceleration during the March 2015 and 2013 storms: The role of ultra-low frequency wave transport from a dynamic outer boundary, Journal of Geophysical Research: Space Physics, 125, e2019JA027 179, 2020.

Palmroth, M., Grandin, M., Sarris, T., Doornbos, E., Tourgaidis, S., Aikio, A., Buchert, S., Clilverd, M. A., Dandouras, I., Heelis, R., Hoffmann, A., Ivchenko, N., Kervalishvili, G., Knudsen, D. J., Kotova, A., Liu, H.-L., Malaspina, D. M., March, G., Marchaudon, A., Marghitu, O., Matsuo, T., Miloch, W. J., Moretto-Jørgensen, T., Baloukidis, D., Olsen, N., Papadakis, K., Pfaff, R., Pirnaris, P., Siemes, C., Stolle, C., Suni, J., van den IJssel, J., Verronen, P. T., Visser, P., and Yamauchi, M.: Lower-thermosphere–ionosphere (LTI) quantities: current status of measuring techniques and models, Annales Geophysicae, 39, 189–237, https://doi.org/10.5194/angeo-39-189-2021, 2021.

Peterson, W. K., Maruyama, N., Richards, P., Erickson, P. J., Christensen, A. B., and Yau, A. W.: What Is the Altitude of Thermal Equilibrium?, Geophysical Research Letters, 50, e2023GL102 758, 2023.

Pfaff, R., Rowland, D., Heelis, R., Clemmons, J., Kepko, L., Thayer, J., Benna, M., and Mesarch, M.: The Atmosphere-Space Transition Region Explorer (ASTRE)–A Low Perigee Satellite to Investigate the Coupling of the Earth's Upper Atmosphere and Magnetosphere, Tech. rep., NASA/TP-20220018963, 2022.

Pirnaris, P. and Sarris, T.: Analysis of in situ measurements of electron, ion and neutral temperatures in the lower thermosphere–ionosphere, Annales Geophysicae, 41, 339–354, https://doi.org/10.5194/angeo-41-339-2023, 2023.

Prikryl, P., Ghoddousi-Fard, R., Weygand, J., Viljanen, A., Connors, M., Danskin, D., Jayachandran, P., Jacobsen, K., Andalsvik, Y., Thomas, E., et al.: GPS phase scintillation at high latitudes during the geomagnetic storm of 17–18 March 2015, Journal of Geophysical Research: Space Physics, 121, 10–448, 2016.

Randall, C., Harvey, V., Singleton, C., Bailey, S., Bernath, P., Codrescu, M., Nakajima, H., and Russell III, J.: Energetic particle precipitation effects on the Southern Hemisphere stratosphere in 1992–2005, Journal of Geophysical Research: Atmospheres, 112, 2007.

Richmond, A.: Ionospheric Electrodynamics Using Magnetic Apex Coordinates, Journal of geomagnetism and geoelectricity, 47, https://doi.org/10.5636/jgg.47.191, 1995.

Richmond, A. and Kamide, Y.: Mapping electrodynamic features of the high-latitude ionosphere from localized observations: Technique, Journal of Geophysical Research: Space Physics, 93, 5741–5759, 1988.

Ridley, A., Deng, Y., and Tóth, G.: The global ionosphere–thermosphere model, Journal of Atmospheric and Solar-Terrestrial Physics, 68, 839–864, 2006.

Roble, R.: The Upper Mesosphere and Lower Thermosphere: A Review of Experiment and Theory, Geophysical Monograph Series, Vol. 87, 1995.

Sarris, T., Palmroth, M., Aikio, A., Buchert, S. C., Clemmons, J., Clilverd, M., Dandouras, I., Doornbos, E., Goodwin, L. V., Grandin, M., Heelis, R., Ivchenko, N., Moretto-Jørgensen, T., Kervalishvili, G., Knudsen, D., Liu, H.-L., Lu, G., Malaspina, D. M., Marghitu, O., Maute, A., Miloch, W. J., Olsen, N., Pfaff, R., Stolle, C., Talaat, E., Thayer, J., Tourgaidis, S., Verronen, P. T., and Yamauchi, M.: Plasma-neutral interactions in the lower thermosphere-ionosphere: The need for in situ measurements to address focused questions, Frontiers in Astronomy and Space Sciences, 9, https://doi.org/10.3389/fspas.2022.1063190, 2023a.

https://doi.org/10.5194/egusphere-2025-4315
Preprint. Discussion started: 17 September 2025

Sarris, T. E.: Understanding the ionosphere thermosphere response to solar and magnetospheric drivers: status, challenges and open issues, Philosophical Transactions of the Royal Society A: Mathematical, Physical and Engineering Sciences, 377, 20180 101, https://doi.org/10.1098/rsta.2018.0101, 2019.

Sarris, T. E., Talaat, E. R., Palmroth, M., Dandouras, I., Armandillo, E., Kervalishvili, G., Buchert, S., Tourgaidis, S., Malaspina, D. M., Jaynes, A. N., Paschalidis, N., Sample, J., Halekas, J., Doornbos, E., Lappas, V., Moretto Jørgensen, T., Stolle, C., Clilverd, M., Wu, Q., Sandberg, I., Pirnaris, P., and Aikio, A.: Daedalus: a low-flying spacecraft for in situ exploration of the lower thermosphere–ionosphere, Geoscientific Instrumentation, Methods and Data Systems, 9, 153–191, https://doi.org/10.5194/gi-9-153-2020, 2020.

Sarris, T. E., Tourgaidis, S., Pirnaris, P., Baloukidis, D., Papadakis, K., Psychalas, C., Buchert, S. C., Doornbos, E., Clilverd, M. A., Verronen, P. T., Malaspina, D., Ahmadi, N., Dandouras, I., Kotova, A., Miloch, W. J., Knudsen, D., Olsen, N., Marghitu, O., Matsuo, T., Lu, G., Marchaudon, A., Hoffmann, A., Lajas, D., Strømme, A., Taylor, M., Aikio, A., Palmroth, M., Heelis, R., Ivchenko, N., Stolle, C., Kervalishvili, G., Moretto-Jørgensen, T., Pfaff, R., Siemes, C., Visser, P., van den Ijssel, J., Liu, H.-L., Sandberg, I., Papadimitriou, C., Vogt, J., Blagau, A., and Stachlys, N.: Daedalus MASE (mission assessment through simulation exercise): A toolset for analysis of in situ missions and for processing global circulation model outputs in the lower thermosphere-ionosphere, Frontiers in Astronomy and Space Sciences, 9, https://doi.org/10.3389/fspas.2022.1048318, 2023b.

Schunk, R. and Nagy, A.: Ionospheres: physics, plasma physics, and chemistry, Cambridge university press, 2009.

Sinnhuber, M., Nieder, H., and Wieters, N.: Energetic particle precipitation and the chemistry of the mesosphere/lower thermosphere, Surveys in Geophysics, 33, 1281–1334, 2012.

Solomon, S. C. and Qian, L.: Solar extreme-ultraviolet irradiance for general circulation models, Journal of Geophysical Research: Space Physics, 110, 2005.

Tesema, F., Partamies, N., Tyssøy, H. N., Kero, A., and Smith-Johnsen, C.: Observations of electron precipitation during pulsating aurora and its chemical impact, Journal of Geophysical Research: Space Physics, 125, e2019JA027 713, 2020.

Tian, X., Yu, Y., and Yue, C.: Statistical survey of storm-time energetic particle precipitation, Journal of Atmospheric and Solar-Terrestrial Physics, 199, 105 204, 2020.

Tourgaidis, S. and Sarris, T.: Wave-particle interactions toolset: A python-based toolset to model wave-particle interactions in the magnetosphere, Frontiers in Astronomy and Space Sciences, 9, 1005 598, 2022.

Tourgaidis, S., Baloukidis, D., Pirnaris, P., Sarris, T., Ridley, A., and Lu, G.: Globally-and Hemispherically-Integrated Joule heating rates during the 17 March 2015 geomagnetic storm, according to Physics-based and Empirical Models, EGUsphere, 2025, 1–27, 2025a.

Tourgaidis, S., Sarris, T. E., Baloukidis, D., Pirnaris, P., and Papadakis, K.: Storm-time Energy Transfer Between Species in the High Latitude Lower Thermosphere-Ionosphere, https://doi.org/10.5281/zenodo.16993754, 2025b.

Turunen, E., Verronen, P. T., Seppälä, A., Rodger, C. J., Clilverd, M. A., Tamminen, J., Enell, C.-F., and Ulich, T.: Impact of different energies of precipitating particles on NOx generation in the middle and upper atmosphere during geomagnetic storms, Journal of Atmospheric and Solar-Terrestrial Physics, 71, 1176–1189, 2009.

Vasyliūnas, V. M. and Song, P.: Meaning of ionospheric Joule heating, Journal of Geophysical Research: Space Physics, 110, https://doi.org/10.1029/2004JA010615, 2005.

Verkhoglyadova, O., Meng, X., Mannucci, A. J., Tsurutani, B. T., Hunt, L. A., Mlynczak, M. G., Hajra, R., and Emery, B. A.: Estimation of energy budget of ionosphere-thermosphere system during two CIR-HSS events: observations and modeling, Journal of Space Weather and Space Climate, 6, A20, 2016.

https://doi.org/10.5194/egusphere-2025-4315
Preprint. Discussion started: 17 September 2025

Verkhoglyadova, O., Meng, X., Mannucci, A., Mlynczak, M., Hunt, L., and Lu, G.: Ionosphere-thermosphere energy budgets for the ICME storms of March 2013 and 2015 estimated with GITM and observational proxies, Space Weather, 15, 1102–1124, 2017.

Verronen, P., Andersson, M., Kero, A., Enell, C.-F., Wissing, J., Talaat, E., Kauristie, K., Palmroth, M., Sarris, T., and Armandillo, E.: Contribution of proton and electron precipitation to the observed electron concentration in October–November 2003 and September 2005, in: Annales Geophysicae, vol. 33, pp. 381–394, Copernicus GmbH Göttingen, Germany, 2015.

Verronen, P., Andersson, M., Marsh, D., Kovács, T., and Plane, J.: WACCM-D—Whole atmosphere community climate model with D-region ion chemistry, Journal of Advances in Modeling Earth Systems, 8, 954–975, 2016.

Vogt, J., Marghitu, O., Blagau, A., Pick, L., Stachlys, N., Buchert, S., Sarris, T., Tourgaidis, S., Balafoutis, T., Baloukidis, D., et al.: Daedalus Ionospheric Profile Continuation (DIPCont): Monte Carlo studies assessing the quality of in situ measurement extrapolation, Geoscientific Instrumentation, Methods and Data Systems, 12, 239–257, 2023.

Wei, D., Yu, Y., and He, F.: The magnetospheric driving source of double-peak subauroral ion drifts: Double ring current pressure peaks, Geophysical Research Letters, 46, 7079–7087, 2019.

Weimer, D.: Improved ionospheric electrodynamic models and application to calculating Joule heating rates, Journal of Geophysical Research: Space Physics, 110, 2005.

Wu, C.-C., Liou, K., Lepping, R. P., Hutting, L., Plunkett, S., Howard, R. A., and Socker, D.: The first super geomagnetic storm of solar cycle 24:"The St. Patrick's day event (17 March 2015)", Earth, Planets and Space, 68, 1–12, 2016.

Yue, X., Wan, W., Liu, L., Liu, J., Zhang, S., Schreiner, W. S., Zhao, B., and Hu, L.: Mapping the conjugate and corotating storm-enhanced density during 17 March 2013 storm through data assimilation, Journal of Geophysical Research: Space Physics, 121, 12–202, 2016.

Zakharenkova, I., Astafyeva, E., and Cherniak, I.: GPS and GLONASS observations of large-scale traveling ionospheric disturbances during the 2015 St. Patrick's Day storm, Journal of Geophysical Research: Space Physics, 121, 12–138, 2016.

Zhang, S.-R., Erickson, P. J., Zhang, Y., Wang, W., Huang, C., Coster, A. J., Holt, J. M., Foster, J. F., Sulzer, M., and Kerr, R.: Observations of ion-neutral coupling associated with strong electrodynamic disturbances during the 2015 St. Patrick's Day storm, Journal of Geophysical Research: Space Physics, 122, 1314–1337, 2017.

Zou, S., Moldwin, M. B., Ridley, A. J., Nicolls, M. J., Coster, A. J., Thomas, E. G., and Ruohoniemi, J. M.: On the generation/decay of the storm-enhanced density plumes: Role of the convection flow and field-aligned ion flow, Journal of Geophysical Research: Space Physics, 119, 8543–8559, 2014.